Phys Chem Minerals (1985) 12:39–44

PHYSICS AND CHEMISTRY OF MINERALS

Transmission Electron Microscope Study of Dislocations in Orthopyroxene $(Mg, Fe)_2 Si_2O_6$

J.C. Van Duysen*, N. Doukhan and J.C. Doukhan
Laboratoire de Structure et Propriétés de l'Etat Solide**, Université de Lille I, 59655 Villeneuve d'Ascq Cédex, France

Abstract. The orthopyroxene crystal structure can be viewed as the stacking of alternating tetrahedral and octahedral layers parallel to the (100) plane. Easy glide occurs in the (100) plane at the level of the octahedral layer to prevent breakage of the strong Si–O bonds. Dislocations with **c** and **b** Burgers vectors have been activated in (100) by room temperature indentation in an orthoenstatite gem quality single crystal. Investigations in transmission electron microscopy show that the **b** dislocations ($b \simeq 9$ Å) are not dissociated while the **c**'s ($c = 5.24$ Å) are dissociated into four partials. This result is interpreted by considering the oxygen sublattice as a distorted FCC one. The four **c** partials are thus Shockley partials bounding three stacking faults. For the two outer ones, synchroshear of the cations is necessary to keep unchanged their sixfold coordination; the oxygen sublattice is locally transformed into a HCP lattice. This accounts for the observed low splitting ($\simeq 100$ Å) of these faults as compared to the median one ($\simeq 500$ Å) which does not affect the oxygen sublattice and does not require cation synchroshear.

In a Fe rich orthopyroxene (eulite), semi coherent exsolution lamellae have been studied. Either only **c** edge dislocations or both **b** and **c** edge dislocations occur in the phase boundaries depending upon the thickness of the lamellae. Only the **c** dislocations are dissociated. From the observed spacing between these mismatch dislocations a crude estimate of the exsolution temperature is proposed $T_{ex} \simeq 700°$ C.

Introduction

Orthopyroxene, $(Mg, Fe)_2Si_2O_6$, chemically a solid solution the end members of which are enstatite, $Mg_2Si_2O_6$ and ferrosilite, $Fe_2Si_2O_6$ is structurally a single chain silicate with *Pbca* as space group. The lattice parameters, which vary slightly with chemical composition, are approximately $a \simeq 18.2$ A, $b \simeq 9$ A and $c \simeq 5.2$ A. The crystallographic structure and the crystal chemistry properties of this material are well known (see recent and detailed reviews on pyroxenes in Deer et al. 1978, Cameron and Papike 1980, 1981). For our purpose which is the discussion of the dislocation structures and the dislocation glide mechanisms, a simplified view of the crystal structure is sufficient in most cases. As suggested by Papike et al. (1973), the oxygen sublattice of pyroxenes is viewed as a more or less distorted compact lattice (FCC or HCP) with the cations in tetrahedral (Si) or octahedral (Mg and Fe) sites. All the pyroxene structures are stackings of alternating tetrahedral and octahedral layers parallel to (100). In the octahedral layers one third of the octahedral sites are empty. Another third comprises the occupied M_1 sites which are fairly regular. The last third (M_2 sites) can be strongly distorted and in some pyroxenes – especially in Ca rich clinopyroxenes – the M_2 cations can be viewed as eightfold coordinated. The distance between M_1 or M_2 cations and the Si cations of the adjacent tetrahedral layers is larger than the corresponding distance for the empty sites. This is probably one of the reasons why these sites cannot be occupied. The tetrahedral layers are formed of chains of corner-sharing SiO_4 tetrahedra. All the chains are parallel to the **c** axis (see Fig. 1).

As Si–O bonds are known to be the strongest ones in silicate structures, easy glide in pyroxenes should occur in (100), in the octahedral layers, in the glide directions (Burgers vectors) **b** and **c**. Furthermore as the structure of this octahedral layer does not change appreciably (except for the cationic composition) in the various pyroxenes, similar defect structures and mechanical properties are expected and it should be possible to relate their variations to chemical changes. In experimentally deformed Mg rich orthopyroxenes, only (100) [001] glide has been characterized (Turner et al. 1960, Raleigh 1965, Green and Radcliffe 1972) while dislocations with [010] as Burgers vector have also been occasionaly observed in naturally deformed crystals (Lally et al. 1972, Kohlstedt and Vandersande 1973). In both cases unit dislocations as well as stacking faults on (100) have been observed with dramatic variations in the ribbon widths from one fault to the next.

The deformation mechanism which has been most studied is the ortho-to clinoenstatite inversion (Turner et al. 1960, Raleigh et al. 1971, Coe and Muller 1973, Boland 1974, Coe and Kirby 1975, Kirby 1976, McLaren and Etheridge 1976). This is a martensitic type transformation which involves partial dislocations gliding in adjacent (100) planes. Depending upon the deformation conditions (temperature and strain rate) orthoenstatite would deform either by dislocation glide or by inversion into clinoenstatite.

Exsolution is another phenomenon which could be related to deformation (Boland 1974, Kirby and Etheridge 1981). At high temperature and high pressure orthoenstatite can dissolve a few percent of calcium which exsolves at lower temperature in thin lamellae of Ca rich clinopyroxene. Exsolution lamellae have been extensively studied in electron microscopy (see reviews in Champness and Lorimer 1976, and Buseck et al. 1980).

* *Present address:* EDF, Centre des Matériaux, 77250 Moret sur Loing, France
** Associated to CNRS no 234

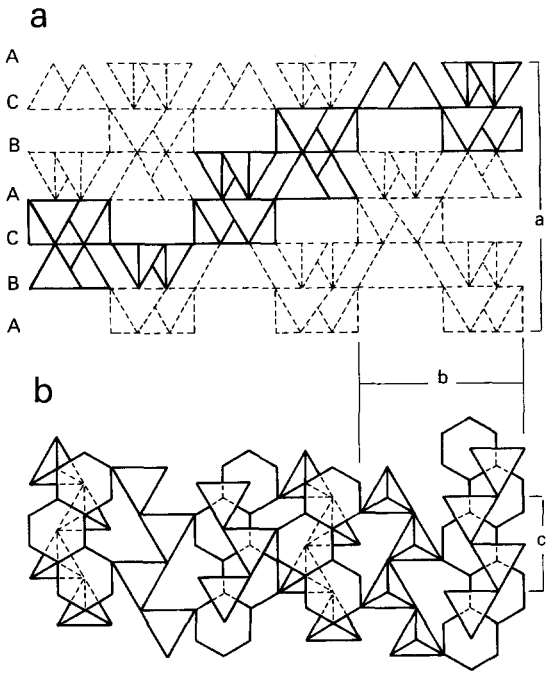

Fig. 1a, b. Schematic view of the orthopyroxene structure *Pbca*. (**a**) Projection on (001), the chains of corner sharing SiO_4 tetrahedra and the chains of edge sharing M_1O_6 octahedra forming the so called I beam structures are shown. The oxygen sublattice is represented here as an undistorted FCC lattice. The stacking sequence of the compact planes ABC ABC is indicated on the left. (**b**) Projection on the (100) plane. Only a part of the structure corresponding to the one in solid lines on a) has been drawn in order to simplify the drawing

In all the above phenomena, dissociated dislocations are expected to play an important role.

Dislocations Induced by Indentation

Indentation is a conventional test for hardness measurements; it can be coupled with *transmission electron microscopy* (TEM) which allows a direct characterization of the activated glide systems and of the core structure of the mobile dislocations. Indentation roughly corresponds to a localized compression at a high strain rate ($\dot{\varepsilon} \simeq 10^{-2}\ s^{-1}$) under appreciable confining pressure (20–30 kb, Gilman 1973). Microhardness tests have been successfully used to investigate the mechanical properties of a variety of hard materials. Further TEM investigations have been performed on some minerals and ceramics like sapphire (Hockey 1973), spinels (Veyssiere et al. 1978, Doukhan 1979), quartz (Trepied and Doukhan 1982), andalusite (Lefebvre 1982), α spodumene (Van Duysen and Doukhan 1983). Schematically the method consists in making, on a well polished surface, numerous microindentations with a moderate load (0.1 to 0.3 N for a Vickers diamond) and then thinning the sample from the opposite face (mechanical thinning down to 30 μm then ion thinning down to a working thickness for TEM observations). An alternative method which has been used for α spodumene consists in gently scratching the polished surface. The motion of the pyramidal diamond along the scratch develops stresses over a wider volume than static indentation. In general less fractures and larger dislocation loops result. We have used this latter process on a gem quality enstatite single crystal from Tanzania with a mean chemical composition

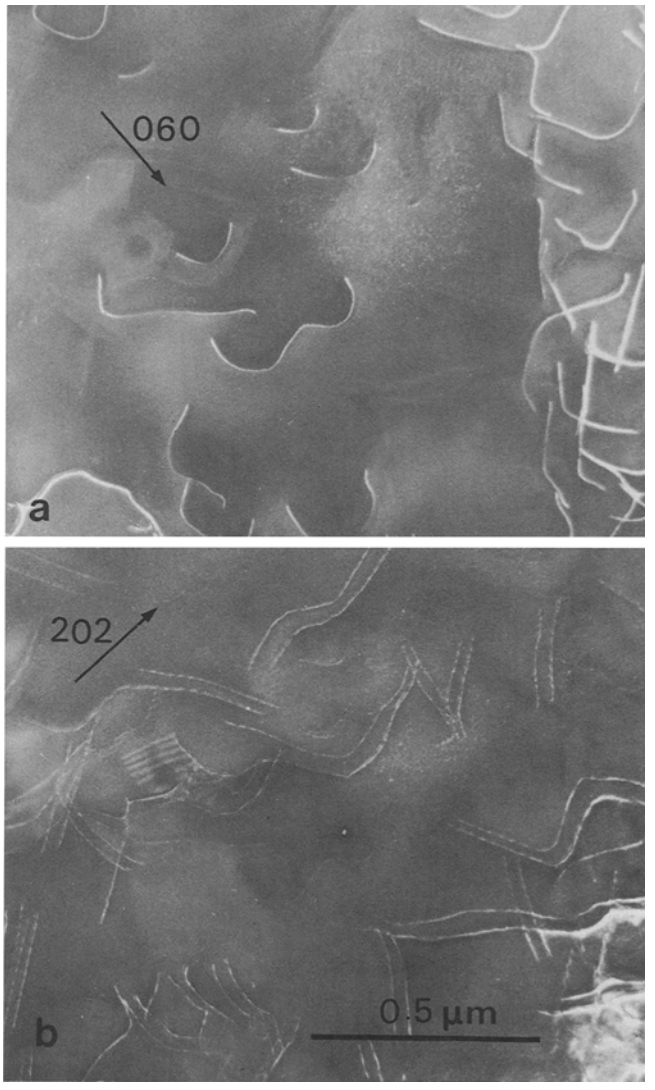

Fig. 2a, b. Scratched orthoenstatite; (301) foil. (**a**) Only **b** dislocations are in contrast with $\mathbf{g}=(060)$ these dislocations are confined in their (100) glide plane and are not dissociated. (**b**) Same area as (**a**) the **b** dislocations are out of contrast while the **c**'s are visible with $\mathbf{g}=(202)$. These latter dislocations also lie in (100) and they are dissociated into four partials. The median ribbon with a width of the order of 500 Å is clearly seen

$Mg_{1.8}Fe_{0.2}Si_2O_6$. It has been verified that the initial dislocation density was very low ($<10^5\ cm^{-2}$). The scratched surface was parallel to (301) i.e. the expected easy glide plane (100) was at 45° to the surface.

In TEM one observes that both (100) [001] and (100) [010] glide systems have been activated. Comparable numbers of **b** and **c** dislocations have been induced and they have glided to similar distances from the scratches. Figure 2 is typical of the observed configurations. As mentioned by previous authors (Kohlstedt and Vandersande 1973, McLaren and Etheridge 1976) the conventional criteria of no contrast for $\mathbf{g}\cdot\mathbf{b}=0$ and $\mathbf{g}\cdot(\mathbf{b}\wedge\mathbf{u})=0$ lead to unambiguous Burgers vector characterizations. We find that the **b** dislocations are out of contrast for $\mathbf{g}=(202)$ and $(20\bar{2})$ reflexions and the **c**'s for $\mathbf{g}=(020)$ and (440). Both **b** and **c** dislocations are well confined in their (100) glide plane which is the only one activated by room temperature indentation. The **b** dislocations are not dissociated while the **c**'s are dissociated into four partials bounding three

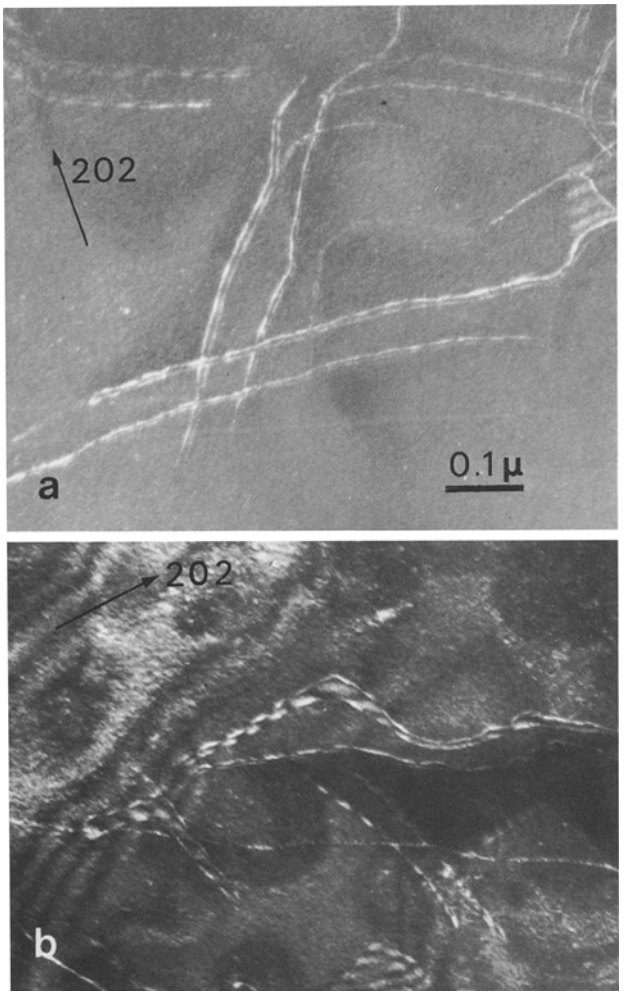

Fig. 3a, b. **c** dislocations produced by scratching. (**a**) Dissociation into four partials bounding three stacking faults. The external narrow ribbons are 100 Å wide approximately. (**b**) In some places, because of the image forces, one of these narrow ribbons widens enough to allow a fringe pattern to be observed

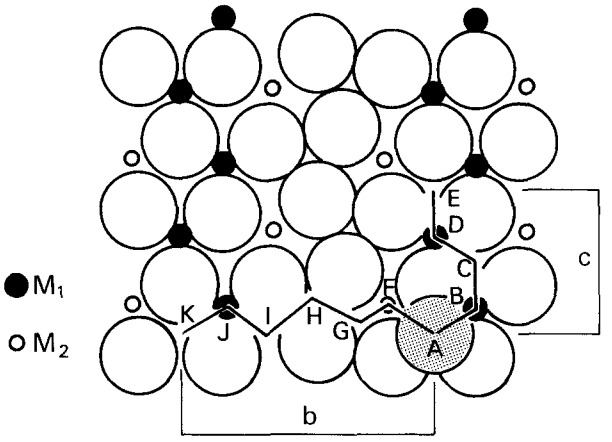

Fig. 4. Propsed dissociation model for the **c** dislocations into four Shockley partials. This view represents the lower (fixed) oxygen layer and only one atom of the upper (mobile) oxygen layer (*dashed circle*). A perfect **c** dislocation would translate the upper layer from A to E. A first dissociation AE = AC + CE would not affect the oxygen sublattice (except for the deviations from perfect FCC lattice) and would keep unchanged the sixfold coordination of the Mg cations. The corresponding stacking fault is expected to be low and a large dissociation width should result (median fault). A further dissociation AC = AB + BC (and correspondingly CE = CD + DE for the other partial) changes the FCC lattice into a HCP one while the Mg cations would become tetrahedraly coordinated. A synchroshear of these cations BC must thus accompany this new dissociation. The associated fault is expected to be larger than the previous one and a narrower ribbon results

stacking faults. The median fault is the widest one (order of 500 Å) and its associated fault vector is $\mathbf{R}_2 = [0, v, 1/2]$ (the fault lies in the (100) plane and exhibits no fringe pattern for the $\mathbf{g} = (202)$ and $(20\bar{2})$ reflexions). The external narrower faults are 100 Å wide approximately (Fig. 3) but in some places the dissociated dislocations lie very near to the surface and image forces split it in such a way that fringe patterns can be observed in one of the narrow ribbons (Fig. 3b). However with the actual thin sample orientation, (202) and $(20\bar{2})$ are the only available reflexions with an extinction distance small enough to allow fringe patterns to be observed. We have thus been unable to fully characterize by diffraction contrast experiments the three fault vectors; only some of their components are known i.e. $\mathbf{R}_1 = [0, \beta, \gamma]$, $\mathbf{R}_2 = [0, v, 1/2]$ and $\mathbf{R}_3 = [0, -\beta - v, 1/2 - \gamma]$. Various extended defects in (100) exhibiting fringe pattern contrast have already been observed and associated with dissociated **c** dislocations (Kohlstedt and Vandersande 1973, Kirby 1976, McLaren and Etheridge 1976). In some cases these extended defects have been assumed to be the premonitory stage of the ortho-to clinoenstatite inversion (Kirby 1976, McLaren and Etheridge 1976). In the present case of room temperature indentation there is no evidence of inversion and the faults are much more narrow than the ones previously observed (in othopyroxenes deformed at high temperature). It thus appears that for these **c** dislocations several dissociation modes can occur depending upon the deformation conditions.

We have looked for low energy stacking faults which can be produced without severe structural reorganization (especially atomic diffusion is insignificant at room temperature). If one assumes as a first approximation that the oxygen sublattice is a FCC one, the simplest dissociation mode for the **c** dislocations would be a dissociation into four Shockley partials, by close analogy with the case of other compact FCC structures (Amelinckx 1982). A first dissociation AE = AC + CE (Figure 4) does not affect the anionic sublattice and the divalent cations keep unchanged their six fold coordination. Their distances to neighbouring Si cations are also unaffected. This leads to the median fault with a low fault energy and a correspondingly large dissociation width. The associated fault vector is $\mathbf{R}_2 = [0, 1/6, 1/2]$. These partials can redissociate into Shockley partials following the reactions AC → AB + BC and CE → CD + DE. This locally changes the FCC anionic sublattice into a hexagonal one and the divalent cations would become tetrahedrally coordinated. To avoid this change in coordination, cations must move synchronously with the oxygen ions as the further dissociations occur. This process is known as synchroshear (Kronberg 1957). As the upper oxygen layer is translated by AB, thus creating the stacking fault with a HCP structure for the oxygen sublattice, the divalent cations move along a route BC to keep unchanged their sixfold coordination. During the dislocation glide, the further translation BC of the upper oxygen layer restores the FCC anionic sublattice and it is accompanied by another cation synchroshear CD. Such a mechanism has been propsed for various oxides with compact oxygen sublattices like corundum (Kronberg 1957), spinels (Hornstra 1960).

With this model the fault vectors would be $\mathbf{R}_1=[0, 0, 1/3]$, $\mathbf{R}_2=[0, 1/6, 1/2]$ and $\mathbf{R}_3=[0, \bar{1}/6, 1/6]$. In fact the oxygen sublattice is distorted and these distortions slightly affect the fault vector components. A drawing of the real octahedral layer (Figure 4) shows that the third component of $\mathbf{R}_1$ could be nearer to 1/4 than to 1/3. It is to be noted that owing to the synchroshear process the distance between the divalent cations and their Si nearest neighbours is never modified; also the spatial distribution in the octahedral layer of empty sites and M_1 and M_2 cations is not affected by the faults. One also notes that the fault widths induced by room temperature indentation do not vary from fault to fault and are at least one order of magnitude narrower than the faults observed in orthopyroxenes strained at high temperature (Kohlstedt and Vandersande 1973, Kirby 1976, McLaren and Etheridge 1976).

It is well known that the elastic energy of a perfect dislocation is proportinal to $|\mathbf{b}|^2$, the square of its Burgers vector, and that dissociation leads to a drastic decrease of this energy with an energy gain of the order of 40%. The previous crystallographic analysis thus raises the following question: why the **b** dislocations which have a larger Burgers vector do not dissociate into Shockley partials like the **c**'s do? This should lead to an appreciable gain of elastic energy and thus to a much more stable configuration. In fact, the structure of the stacking fault as well as the elastic energy have to be considered for each dissociation. A dissociation AK = AF + FG + GH + HI + IJ + JK (Fig. 4) would be constituted of three partials AF, GH and IJ transforming the FCC anionic sublattice into a hexagonal one while the three other partials would restore the FCC sublattice. Cationic synchroshear would accompany these dissociations but in the case of **b** dislocations, cations would necessarily move into the empty sites and their distances to nearest Si neighbours would be shortened. Larger stacking fault energies would probably result and this could be the reason why **b** dislocations do not dissociate. In α spodumene which is a monoclinic pyroxene it has been found that **b** dislocations can be dissociated into two partials (Van Duysen and Doukhan 1983) but the crystallographic analysis of the fault suggests that there is no cationic synchroshear in this case. The Al cations would become tetrahedrally coordinated, leading to a layer of another polymorph, γ spodumene. A somewhat similar argument could hold for the observed variations in the dissociation widths of **c** dislocations if these dissociations are the premonitory stage of a polymorphic transformation (ortho to clino inversion).

Mismatch Dislocations

When orthopyroxenes cool from the igneous or metamorphic conditions at which they have formed they exsolve a Ca rich monoclinic phase which preferentially nucleates on lattice defects as thin lamellae parallel to (100) planes of the matrix. Exsolution lamellae in orthopyroxenes, especially in Mg rich ones have already been carefully investigated by analytical TEM (for a recent review, see Buseck et al. 1980). We have studied the epitaxial relations and the mismatch dislocations occurring at the interphase boundaries in a Fe-rich orthopyroxene from St. Paul, Labrador, Canada. The mean chemical composition of the matrix is $Mg_{0.48}\,Fe_{1.50}\,Ca_{0.02}\,Si_2O_6$ (eulite) and semi quantitative analysis of the lamellae lead to $Mg_{0.3}\,Fe_{0.9}\,Ca_{0.8}\,Si_2O_6$ (sub calcic hedenbergite). These latter appear in TEM

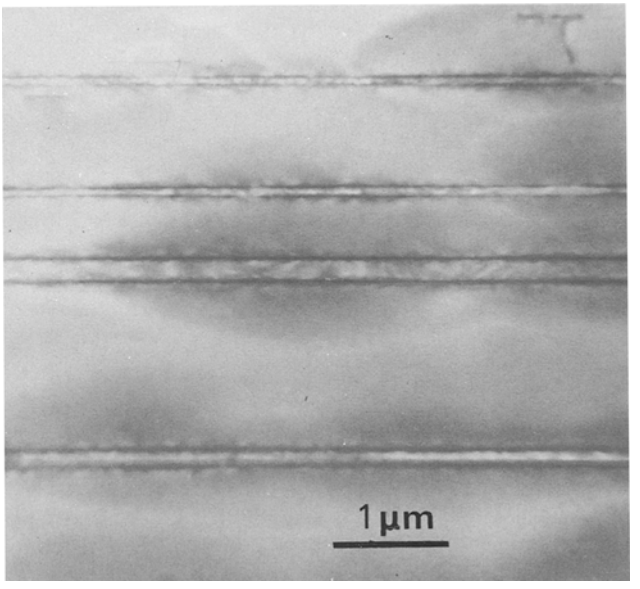

Fig. 5. Exsolution lamellae in a Fe rich pyroxene from Labrador (Canada), (010) foil. The lamellae are typically 1,000 Å wide and from one to a few microns apart. They are parallel to the (100) matrix plane

as thin (typically 1,000 Å) lamellae parallel to the (100) matrix plane and one to a few microns apart (Fig. 5). From electron diffraction patterns (Fig. 6) the following epitaxial relations are found: $\mathbf{b}_m \| \mathbf{b}_l$ and $\mathbf{c}_m \| \mathbf{c}_l$ where m and l indices stand for matrix and lamella respectively. The spacing of the mismatch dislocations (Fig. 7) is consistent with the lattice parameter differences that existed at the exsolution temperature if no further reorganisation in the phase boundary occurred during cooling. At room temperature one has on the one hand the reference values taking into account the chemical composition:

* subcalcic hedenbergite lamella: $a=9.80$ Å; $b=9.01$ Å; $c=5.24$ Å; $\beta=105.5°$ (Cameron et al. 1973, Cameron and Papike 1980)
* eulite matrix: $a=18.40$ Å; $b=9.03$ Å; $c=5.24$ Å (Smith et al. 1969).

On the other hand, precise measurements on electronic diffraction patterns lead to the following values for the lamella (the diffraction constant of the microscope is calibrated with the above values for eulite): $a'=9.72\pm0.01$ Å; $b'=8.99\pm0.03$ Å; $c'=5.27\pm0.01$ Å; $\beta'=105\ 3/4\pm1/4°$. This means that lamellae are now elastically strained i.e. the mismatch dislocation configuration is frozen from some temperature equal or lower to the exsolution temperature T_{ex}. A crude estimate of a lower limit for T_{ex} can be found as follows. Neglecting the influence of pressure, the high temperature equilibrium of lamella and matrix with their epitaxial relations and their different lattice parameters was such that n lattice plane of the lamella $\perp c$ had exactly the same thickness as $(n+1)$ (001) lattice planes of the matrix (Fig. 8).

$$n\,c_l\,(T_{ex}) = (n+1)\,c_m\,(T_{ex}) \qquad (1)$$

this means that there would be one extra half plane in the matrix (**c** edge dislocation) every $(n+1)$ (001), plane i.e. the spacing between perfect mismatch dislocations would be $(n+1)\,c_l$. In fact, in the actual case, these **c** dislocations

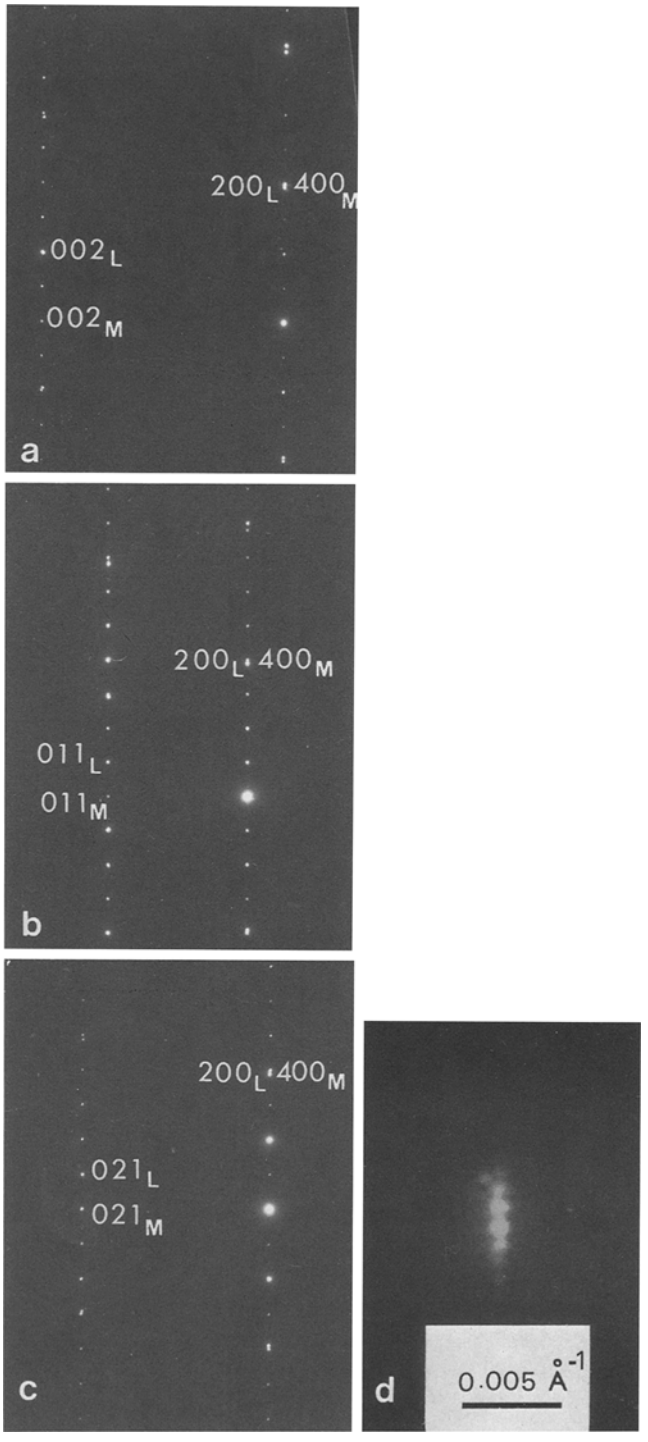

Fig. 6a–d. Diffraction patterns of a selected area enclosing the matrix and a lamella (indices M and L respectively) showing the epitaxial relationships (**a**) $(010)_{\overline{M}}$ section; (**b**) section with $(100)_M$ and $(011)_M$; (**c**) section with $(100)_M$ and $(021)_M$; (**d**) fine structure of a diffraction spot of the lamella

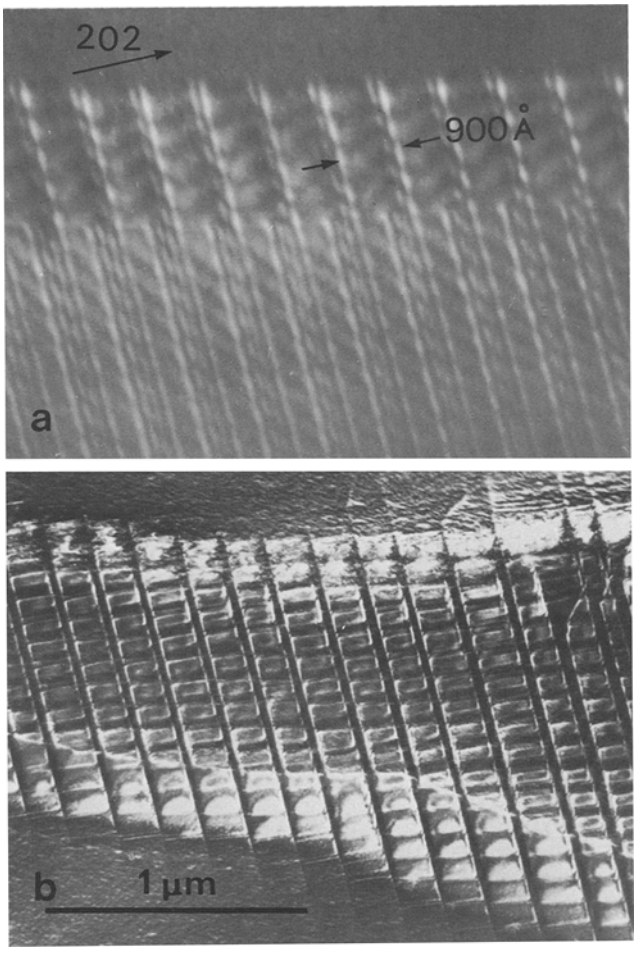

Fig. 7a, b. Semi coherent phase boundaries of a lamella. (**a**) Thin lamella with only **c** edge dislocations dissociated into four partials in the boundaries. Both phase boundaries visible, (**b**) lamella with **b** and **c** edge mismatch dislocations in the phase boundaries

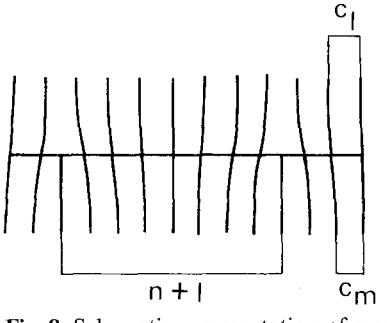

Fig. 8. Schematic representation of a semicoherent boundary with a **c** edge mismatch dislocation every n unit repeats in the lamella and $(n+1)$ unit repeats in the matrix

are dissociated into four Shockley partials and the corresponding stacking fault energies are lower than in the bulk eulite because the material is imperfectly organised in the phase boundary. On Figure 7a n thus corresponds to four dislocations i.e. $n=1800/5.24=344$. Furthermore α_l and α_m being the thermal expension coefficients in the **c** direction of the lamella and the matrix respectively, Equation (1) becomes

$$n\, c_l^0\,(1+\alpha_l\,\Delta T)=(n+1)\, c_m^0\,(1+\alpha_m\,\Delta T) \qquad (2)$$

with $\Delta T=T_{ex}-T_{room}$, c_l^0 and c_m^0 being the lattice parameters at room temperature of the lamella and the matrix respectively. Equation (2) can be rewritten:

$$\frac{n+1}{n}=\frac{c_l^0}{c_m^0}\,\frac{1+\alpha_l\Delta T}{1+\alpha_m\Delta T} \quad \text{or} \quad \frac{1}{n}\simeq(\alpha_l-\alpha_m)\,\Delta T \qquad (3)$$

the α values are $\alpha_l=0.60\ 10^{-5}\ °C^{-1}$ (Cameron et al. 1973) and $\alpha_m=0.17\ 10^{-5}\ °C^{-1}$ (Sueno et al. 1976). With the

above value of $n=344$ one deduces $\Delta T=6$ 75 °C i.e. the observed configuration would have been frozen at 700 °C.

Such an estimate cannot be very precise, not only because the various parameters like n and the α's are not very precisely known but because the basic principle itself is not completely correct. The fitting of two lattices with slightly different lattice periods corresponds to a minimization of the elastic energy. Homogeneous elastic deformation of the lamella is a competitive process which cannot be ignored for small size lamellae. This is clearly shown by comparison of Figures 7a and b. On the first one only mismatch dislocations with **c** as Burgers vector occur in the phase boundary while the lower mismatch along the **b** direction is matched by homogeneous elastic compression in this direction. In contrast, for the bigger lamella shown on Figure 7b both **b** and **c** edge mismatch dislocations occur in the phase boundary (at the end of this lamella, one again finds **c** dislocations only).

Finally it can be remarked that when only **c** edge mismatch dislocations occur, they are present in both phase boundaries. In thin lamellae their strain field induces a spatial modulation of the lamella crystal lattice which exhibits a pseudo "super lattice" with a super period $nc=1800$ Å appearing as a fine structure of the diffraction spots associated with the strained lamella (Fig. 6d).

Conclusion

In orthopyroxenes deformed either naturally or experimentally at high temperature it is very difficult to distinguish true dissociated dislocations from very thin exsolution lamellae or very thin lamellae of inverted enstatite. In room temperature indented specimens it has been possible to clearly show that **c** dislocations are dissociated into four partials which can be compared with Shockley partials in FCC structures. This result allows a crude estimate of the exsolution temperature to be made by examination of the mismatch dislocations occurring at the boundaries of exsolution lamellae. Finally **b** dislocations can be activated in (100) at least at room temperature, and the elastic limit of this glide system can be compared with that of the only known easy glide system of this structure i.e. (100) [001].

References

Amelinckx S (1982) Dislocations in particular structures. In: Nabarro FRN (ed) Dislocations in solids 2. North Holland, Amsterdam, p 67

Boland JN (1974) Lamellar structures in low calcium orthopyroxenes. Contrib Mineral Petrol 47:215–222

Buseck P, Nord GL, Veblen DR (1980) Subsolidus phenomena in pyroxenes. In: Ribbe PH (ed) Reviews in mineralogy 7: Pyroxenes Mineral Soc Am, Washington DC, pp 117–212

Cameron M, Sueno S, Prewitt CT, Papike JJ (1973) High temperature crystal chemistry of acmite, diopside, hedenbergite, jadeite, spodumene and ureyite. Am Mineral 58:594–618

Cameron M, Papike JJ (1980) Crystal Chemistry of silicate pyroxenes. In: Ribbe PH (ed) Reviews in mineralogy 7: Pyroxenes. Mineral Soc Am, Washington DC, pp 5–92

Cameron M, Papike JJ (1981) Structural and chemical variations in pyroxenes. Am Mineral 66:1–50

Champness PE, Lorimer GW (1976) Exsolution in silicates. In: Wenk HR (ed) Electron microscopy in mineralogy, Springer, Berlin Heidelberg New York, pp 174–204

Coe RS, Muller WF (1973) Crystallographic orientation of clinoenstatite produced by deformation of orthoenstatite. Science 180:64–66

Coe RS, Kirby SH (1975) The orthoenstatite to clinoenstatite transformation by shearing and reversion by annealing: mechanisms and potential applications. Contrib Mineral Petrol 52:29–55

Deer WA, Howie RA, Zussman J (1978) Rock forming minerals 2A: Single chain silicates. Wiley, New York

Doukhan N (1979) TEM investigation of room temperature microplasticity in Mg Al_2O_4 spinel. J Phys 40:L 603–L 606

Gilman JJ (1973) Hardness, a strength microprobe. In: Westbrook JK, Conrad H (eds) The science of hardness testing and its research applications. Am Soc Metals, Metals Park Ohio, pp 51–74

Green HW, Radcliffe SV (1972) Deformation processes in the upper mantle. In: Heard HC, Borg LY, Carter NL, Raleigh CB (eds) Flow and fracture of rocks. Am Geophys Union, Washington DC, pp 139–156

Hockey BJ (1973) Use of the hardness test in the study of the plastic deformation of single crystals. In: Westbrook JK, Conrad H (eds) The science of hardness testing and its research applications. Am Soc Metals, Metals Park Ohio, pp 21–50

Hornstra J (1960) Dislocations, stacking faults and twins in the spinel structure. J Phys Chem Solids 15:311–323

Kirby SH (1976) The role of crystal defects in the shear induced transformation of orthoenstatite to clinoenstatite. In: Wenk HR (ed) Electron microscopy in mineralogy. Springer, Berlin Heidelberg New York, pp 465–472

Kirby SH, Etheridge MA (1981) Exsolution of Ca pyroxene from orthopyroxene aided by deformation. Phys Chem Minerals 7:105–109

Kohlstedt DL, Vandersande JB (1973) Transmission electron microscopy investigation of the defect microstructure of four natural orthopyroxenes. Contrib Mineral Petrol 42:169–180

Kronberg ML (1957) Plastic deformation of single crystals of sapphire, basal slip and twinning. Acta Metall 5:507–524

Lally JS, Fisher RM, Christie JM, Griggs DT, Nord NL, Radcliffe SV (1972) Electron petrography of Apollo 14 and 15 rocks. Proc Lunar Sci Conf 3rd:401–422

Lefebvre A (1982) Transmission electron microscopy of andalusite single crystals idented at room temperature. Bull Mineral 105:347–350

McLaren AC, Etheridge MA (1976) A transmission electron microscopy study of naturally deformed orthopyroxene. I Slip mechanisms. Contrib Mineral Petrol 57:163–177

Papike JJ, Prewitt CT, Sueno S, Cameron M (1973) Pyroxenes; comparisons of real and ideal structure topologies. Z Kristallogr 138:252–273

Raleigh CB (1965) Glide mechanisms in experimentally deformed minerals. Science 150:739–541

Raleigh CB, Kirby SH, Carter NL, Ave-Lallemand HG (1971) Slip and the clinoenstatite transformation as competing rate processes in enstatite. J Geophys Res 76/17:4011–4022

Smith JV, Stephenson DA, Howie RA, Hey MH (1969) Relations between cell dimensions, chemical composition and site preference of orthopyroxene. Mineral Mag 37:90–114

Sueno S, Cameron M, Prewitt CT (1976) Orthoferrosilite: high temperature crystal chemistry. Am Mineral 61:38–53

Trepied L, Doukhan JC (1982) Transmission electron microscopy study of quartz single crystals deformed at room temperature and atmospheric pressure by indentation. J Phys 43:L77–L81

Turner FJ, Heard HC, Griggs DT (1960) Experimental deformation of enstatite and accompanying inversion to clinoenstatite. Rpt 21st Int Geol Congr Copenhagen 18:399–408

Van Duysen JC, Doukhan JC (1983) Room temperature microplasticity of α spodumene Li Al Si_2 O_6. Phys Chem Minerals 10:125–132

Veyssiere P, Rabier J, Garem H, Grilhe J (1978) Influence of temperature on dissociation of dislocations and plastic deformation in spinel oxides. Philos Mag 38:61–79

Received March 15, 1984